WATER RESOURCES RESEARCH, VOL. 34, NO. 11, PAGES 3157–3168, NOVEMBER 1998

Rill erosion and morphological evolution: A simulation model

Tingwu Lei and Mark A. Nearing

National Soil Erosion Research Laboratory, Agricultural Research Service, U.S. Department of Agriculture West Lafayette, Indiana

Kamyar Haghighi and Vincent F. Bralts

Agricultural and Biological Engineering Department, Purdue University, West Lafayette, Indiana

Abstract. A mathematical model is advanced to simulate dynamically and spatially varied shallow water flow and soil detachment, transport, and deposition in rills. The model mimics the dynamic process of rill evolution, including variable rates of sediment redistribution along the bed and changes in local bed morphology. The sediment source term in the model uses a point scale, probabilistic relationship based on turbulent flow mechanics and a recently developed sediment transport relationship for rills based on stream power. The interdependent feedback loops between channel bed morphology, local flow hydraulics, and local scour and deposition, within the framework of the full hydrodynamic equations with inertial terms, constitute a mathematical model with the capacity to represent spatial variability and temporal evolution of the rill. Finite elements were applied to numerically solve the hydrodynamic and sediment continuity equations. A series of laboratory flume experiments were performed to evaluate the model. Initial bed slopes were 3, 5, and 7% with step increases of water inflow rates of 7.6, 11.4, and 15.2 L min^{-1}. The soil material used in the flume was a kaolinitic, sandy-clay loam. The rill model equations were solved for increasingly complex cases of spatial and temporal variabilities. The model followed measured patterns of morphological changes as the rill evolved, which suggests that the feedback loops in the model between erosion, bed morphological changes, and hydraulics were adequate to capture the essence of rill evolution.

1. Introduction

Rills are small channels which function as both sediment source areas and sediment transport vehicles on hillslopes. They are therefore critical components to the erosion system for upland areas. Where erosion rates are great, actively eroding rills are generally present [*Ellison*, 1947; *Foster*, 1982; *Gilley et al.*, 1990; *Govers*, 1990, 1992; *Govers and Rauws*, 1986; *Nearing et al.*, 1989, 1997]. Eroding rills evolve morphologically in time and space. The rill bed surface changes as soil erodes, which in turn alters the hydraulics of the flow. The hydraulics is the driving mechanism for the erosion process, and therefore dynamically changing hydraulic patterns cause continually changing erosional patterns in the rill. Thus the process of rill evolution involves a feedback loop between erosion, hydraulics, and bed form. Flow velocity, depth, width, hydraulic roughness, local bed slope, friction slope, and erosion rate are time and space variable functions of the rill evolutionary process. The purpose of this work was to gain a more complete understanding of the evolutionary process of rill development using a combination of theoretical, numerical, and empirical methods. This paper presents the conceptual and mathematical relationships which are used to describe rill erosion processes, numerical solutions of the rill erosion equations, comparisons to measured rill erosion data, and implications of the model result relative to the scientific understanding of erosion.

Paper number 98WR02162.
0043-1397/98/98W-02162$09.00

Current models rely on assumptions and mathematics which simplify the dynamic and spatially varying nature of rill erosion. Such simplifications are made for several reasons, not the least of which is that most erosion models are oriented toward predictions for soil conservation purposes rather than for the scientific understanding of the processes involved. Full descriptions of soil erosion involve complex equations which are often not suited to soil erosion prediction technology and are not warranted in terms of erosion prediction accuracy, since soil erosion is highly variable even under supposedly similar environmental conditions [*Wendt et al.*, 1986]. Current models do not attempt to describe rill evolution and the associated spatially variability in rills. The Water Erosion Prediction Project (WEPP) [*Flanagan and Nearing*, 1995; *Nearing et al.*, 1989, 1990; *Nearing and Nicks*, 1998]; GUEST [*Misra and Rose*, 1996]; Hairsine and Rose [*Hairsine and Rose*, 1992a, b]; and EUROSEM [*Morgan et al.*, 1992; *Morgan*, 1995] models, for example, assume a constant flow width, constant hydraulic roughness, linear changes in flow rates with distance, and a nonchanging slope steepness profile. In addition to these limitations, both WEPP and GUEST are steady state models, and all four have limited capability in addressing spatial variability. All four of these models, as well as several others, are useful for erosion prediction purposes if adequately parameterized, but none attempt to mimic rill evolution.

The objective of this research was to construct a model which mimics the physics of rill evolution. The result is a mathematical model which self-generates the temporal and spatial variability of rill characteristics by linking the processes

of erosion, changes in bed morphology, and hydraulics through dynamic feedback loops. Changes in local rill slope and width are based on the dynamics of local soil detachment and sediment deposition rates. Changes in slope and width cause associated changes in flow velocity, shear stress, and energy, which in turn define the capacity of the flow to detach, transport, and deposit sediment. The model uses a full form of the hydrodynamic routing equations, a probabilistically based soil detachment model, and a new sediment transport equation for rill erosion. Finite element techniques were used to solve the erosion equations. Laboratory experiments were conducted in order to test the model. The experiments involved three (initial) slopes of 3, 5, and 7%, and three nominal levels of water inflow rates of 7.6, 11.4, and 15.2 L min^{-1} at each slope. We performed the study by applying the model through increasing levels of complexity in the description of the rilling process. The first case was essentially that used by rill erosion models to date: both rill widths and bed slopes are considered to be time invariant and spatially uniform through the simulation period. In the second case, widths are time invariant and spatially uniform, whereas slopes are time variable and spatially nonuniform. In this second case we begin to investigate the implications of changing morphology on sediment production in the rill because the slope changes nonuniformly based on nonuniformity in scouring of the bed. In the third case, widths are time invariant but spatially nonuniform, and slopes are again time variable and spatially nonuniform. Finally, we consider the most complex and most realistic case of time variant and spatially nonuniform rill widths and bed slopes.

The model has several limitations, which we list here and discuss in more detail in section 5: (1) Calculations for channel width adjustments are somewhat restrictive due to the one-dimensional treatment of the flow and sediment flux as well as limitations in knowledge of the processes involved. (2) Parameter values, particularly for sediment deposition and dispersion terms, are defined by reasonable model response (sensitivity) rather than by a physical basis. (3) The lack of test data for clear quantification on rates of rill widening and narrowing prohibits the capability for a complete test of the how the model performs as a function of time. (4) The need and lack of physical explanation for the introduction of a minimum flow depth in the hydraulic calculations indicate a gap in the knowledge of this process.

2. Model Description

2.1. Hydrodynamic Equations

One-dimensional hydrodynamic equations for constant width have been discussed extensively [see *Milne-Thomson*, 1960; *Shames*, 1992; *Zienkiewicz and Taylor*, 1991]. This model differs in that the width may be nonuniform and dynamically changing. Using mass balance, the continuity equation for water flow in a width-varied rill is given as

$$\frac{\partial(hw)}{\partial t} + \frac{\partial(uhw)}{\partial x} = \sigma w \tag{1}$$

where x (m) is downslope distance, t (s) is time, $h(x, t)$ (m) is depth of flow measured in the vertical direction, $u(x, t)$ (m s^{-1}) depth- and width-averaged velocity in the x direction, $w(x, t)$ (m) is width of rill, $\sigma(x, t)$ (m s^{-1}) is the addition or subtraction of water mass along the rill such as might occur via rainfall excess, reemergent subsurface flow, or transmission losses.

Momentum conservation gives the following equation for water flow in a width-varied rill [*Jayawardena and White*, 1977]:

$$\frac{\partial(uhw)}{\partial t} + \frac{\partial(u^2hw)}{\partial x} + \frac{g}{2}\frac{\partial(h^2w)}{\partial x} = -ghw\left(\frac{S_x}{\sqrt{1+S_x^2}} + S_{fx}\right) \tag{2}$$

where g (m s^{-2}) is acceleration due to gravity, $S_x(x, t)$ (m m^{-1}) is slope of the rill, $S_{fx}(x, t)$ (m m^{-1}) is friction slope given as [*Chow*, 1959]

$$S_{fx} = \left(\frac{u}{C}\right)^2 \frac{1}{h} \tag{3}$$

where Chezy's C ($m^{1/2}$ s^{-1}) is a factor of flow resistance given by [*Chow*, 1959]

$$C = \sqrt{8g/f} \tag{4}$$

The term f (nondimensional) in (4) is the Darcy-Weisbach hydraulic friction coefficient.

Bed slope is simply

$$S_x = \partial z/\partial x \tag{5}$$

where $z(x, t)$ (m) is the elevation of the ground surface.

2.2. Sediment Continuity Equation

The sediment transport associated with the shallow water flow is given by

$$hw\frac{\partial c}{\partial t} + hwu\frac{\partial c}{\partial x} = \frac{\partial}{\partial x}\left(hwD_x\frac{\partial c}{\partial x}\right) + (S_{ss} - c\sigma)w \tag{6}$$

where $c(x, t)$ (kg m^{-3}) is sediment concentration, $S_{ss}(x, t)$ (kg m^{-2} s^{-1}) is the sediment source/sink term, and D_x (m^2 s^{-1}) is the dispersion coefficient for the sediment. The dispersion term in (6) is not often used in erosion routing equations, data for attaching a value to D_x is limited, and its importance is not well documented. However, the physical presence of the process is certain, particularly for the one-dimensional case. A cross section of the rill flow at any point and at any moment in time will invariably exhibit a distribution of flow velocities. The flow velocity variations are due in part to variations in the cross-sectional geometry of the flow, as well as to differences in flow velocity between the free flowing stream and the fluid boundary layer.

2.3. Sediment Source/Sink Term

Equation (6) for sediment continuity is a relatively noncontroversial equation in erosion literature; however, the form of the source term for (6) is the subject of lively discussion in the field of erosion science [*Elliot*, 1988; *Elliot and Laflen*, 1993; *Elliot et al.*, 1989; *Ellison*, 1947; *Foster*, 1982; *Rose et al.*, 1983a, b; *Hairsine and Rose*, 1992a, b; *Laflen et al.*, 1991; *Morgan et al.*, 1992; *Morgan*, 1995; *Nearing et al.*, 1990; *Meyer et al.*, 1975]. In the development of this erosion model we chose to use the concept of transport capacity, with detachment occurring when sediment load is less than local transport capacity and deposition occurring when sediment load exceeds local transport capacity.

2.3.1. Detachment rate. Soil detachment by flowing water is caused by turbulence [*Nearing and Parker*, 1994]. To date all physically based soil erosion models have used average flow parameters, such as average flow shear stress [*Nearing et al.*,

1989] or unit stream power [*Morgan et al.*, 1995]. In this model we used a detachment model which is based explicitly on the characteristics of intermittent turbulent flow stresses which cause soil detachment. The relationship is presented in detail by *Nearing* [1991]. The relationship for detachment by turbulent flow takes the form

$$e = FPM \tag{7}$$

where e (kg $(m^2\ s)^{-1}$) is detachment rate from the bed, F (s $m^2)^{-1}$ is the spatial and temporal frequency of turbulent "bursts" associated with coherent flow structures, P is the probability that the burst will cause a failure event on the bed which detaches soil, and M (kg) is the average mass detached per failure event. The equation may also be written as [*Nearing*, 1991a]

$$e = KCPh^{1/2}S_{fx}^{3/2} \tag{8}$$

where K is an empirical coefficient which can be determined from experimental data, C is the Chezy roughness coefficient, h (m) is flow depth, and S_{fx} (m m^{-1}) is friction slope. The probability of detachment, P, is equal to the overlapping portion of two distribution functions: the first of the soil tensile strength for individual soil particles which acts as the resistance force to detachment and the second is the instantaneous shear stresses associated with turbulent bursts at the bed surface (Figure 1).

The term e is the potential detachment rate, i.e., the detachment rate for clear water flow. The actual value of the source term, S_{ss}, is calculated based on the potential detachment rate and an adjustment to account for sediment load transport as discussed below in the section 2.3.3.

2.3.2. Sediment transport capacity. The transport capacity relationship for the model was taken from recent laboratory experiments on rills [*Nearing et al.*, 1997]:

$$\log_{10}(T_c) = A + \frac{B \exp[a + b \log(\omega)]}{1 + \exp[a + b \log(\omega)]} \tag{9}$$

where T_c (g $(cm\ s)^{-1}$)) is sediment transport capacity, a = 0.845; b = 0.412; A = −34.47; B = 38.61; and ω (g s^{-3}) is defined as stream power and is given as

$$\omega = \rho g S_{fx} q \tag{10}$$

where q ($cm^2\ s^{-1}$) is the unit flow discharge and ρ (g cm^{-3}) is the density of water.

2.3.3. Detachment/transport coupling. The potential detachment rate e is based on the a model which describes the physics of soil detachment by clear water, turbulent flow. The presence of sediment in the flow will reduce the actual detachment rate due to several factors. One reason for the reduction in soil detachment rate with the presence of sediment in the flow is related to the effect of sediment on turbulent velocity fluctuations. *Einstein Ning Chien* [1954] and *Vanoni and Namicos* [1960] discussed the reduction in turbulent intensities with the presence of sediment in the flow. Another explanation was suggested by *Rose et al.* [1983a, b] and *Hairsine and Rose* [1992a, b], who attribute the effect of sediment load on detachment rates to the shielding of the bed surface by sediments which are continually deposited on the bed and subsequently reintrained during the transport process. A third argument for explaining the interaction of sediment on detachment was presented by *Foster and Meyer* [1972] and *Meyer et al.* [1975], wherein they suggest simply that detachment rate is reduced with the presence of sediment due to the fact that energy expended on transport is not available for detachment.

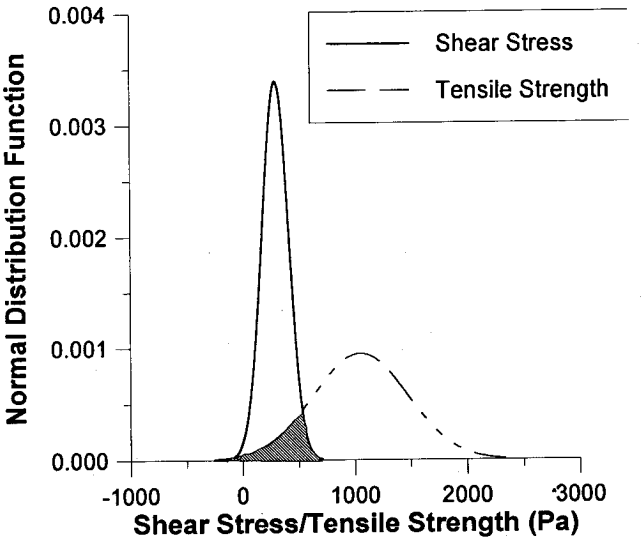

Figure 1. Probability density functions for instantaneous turbulent boundary shear stresses and soil particle tensile strengths (conceptual).

In this model we assumed a linear decrease in detachment rate as a function of sediment load, i.e.,

$$S_{ss} = e\left(1 - \frac{cq}{T_c}\right) \tag{11}$$

2.3.4. Sediment deposition. For the case where sediment load, (cq), is greater than the transport capacity, T_c, deposition is calculated as a first-order process relative to the excess load, i.e.,

$$S_{ss} = -\alpha(cq - T_c) \tag{12}$$

where α (m^{-1}) is an empirical, first-order, deposition coefficient.

2.4. Temporal Evolution of Rill Bed

2.4.1. Elevational changes. The sediment transport capacity at an instant in time will vary spatially in the rill as a function of the stream power, which is itself a function of rill width, depth, flow rate, velocity, and local friction slope. Differences in the sediment transport capacity will in turn effect differences in detachment and deposition rates, as well as changes along the bed from detachment to deposition regimes and vice versa. Thus even in a rill with a uniform initial bed slope and uniform flow rate on a homogeneous soil bed, random variations in rill width can cause variances in transport capacity which cause differences in the source term of the sediment continuity equation.

Local detachment and deposition cause temporal changes in the local bed slope because the rill bed does not erode uniformly. Detachment or deposition during the time period (dt) on the surface area of $(w\ dx)$ cause changes in the sediment mass equal to the term $(S_{ss}w\ dx\ dt)$, and the mass change in sediment on the bed is $-\rho_b(\partial z/\partial t)w\ dt\ dx$, where ρ_b (kg m^{-3}) is the bulk density of soil. Mass balance requires that the sediment source or deposition equal the sediment detached from or deposited on the rill bed, namely,

$$S_{ss} w\, dx\, dt = -\rho_b \frac{\partial z}{\partial t} dt\, w\, dx \tag{13}$$

and

$$\frac{\partial z}{\partial t} = -\frac{1}{\rho_s} S_{ss} \tag{14}$$

Integration of (14) yields

$$z(x, t) = -\frac{1}{\rho_b} \int_{t_0}^{t_0+\Delta t} S_{ss}(x, t)\, dt + z(x, t_0) \tag{15}$$

where $z(x, t_0)$ is the initial morphologic function of the rill bed at the beginning of the time increment.

The case of $S_{ss}(x, t)|_{x=x_1} < 0$ indicates deposition. In that case $z(x, t_0 + \Delta t) > z(x, t_0)$, which means elevation of the rill bed at that point is increasing due to sediment deposition on the surface. For the case of detachment, $z(x, t_0 + \Delta t) < z(x, t_0)$ in combination with $S_{ss}(x, t) > 0$.

2.4.2. Width changes. When deposition occurs in a section of a rill, the slope of upstream side will decrease along with the water depth and velocity. Mass balance requires that the rill width increase. At constant flow rates the mass of water flow remains unchanged therefore from mass balance:

$$u_1 w_1 h_1 = u_2 w_2 h_2 \tag{16}$$

where u_1 and u_2 are fluid velocities, w_1 and w_2 are rill widths, and h_1 and h_2 are water depths at the beginning and the end of a time segment of deposition, with

$$\begin{aligned} u_2 &= u_{t=t_1} + \left(\frac{\partial u}{\partial t}\Delta t\right)\Big|_{t=t_1} = u_1 + \Delta u \\ w_2 &= w|_{t=t_1} + \left(\frac{\partial w}{\partial t}\Delta t\right)\Big|_{t=t_1} = w_1 + \Delta w \\ h_2 &= h|_{t=t_1} + \left(\frac{\partial h}{\partial t}\Delta t\right)\Big|_{t=t_1} = h_1 + \Delta h \end{aligned} \tag{17}$$

where $\Delta t = t_1 - t_0 > 0$.

Here we suggest that a fraction of the total depth of deposited sediment (Δz) contributes to the decrease in water depth, i.e.,

$$h_2 = h_1 + \gamma \Delta z \tag{18}$$

where $0 \le \gamma \le 1$ is the coefficient of water depth decrease due to deposition. The new rill width, w_2, is then given as

$$w_2 = \frac{w_1 h_1}{h_1 + \gamma \Delta z} \tag{19}$$

In the case of deposition, $\Delta z < 0$; thus we can see from (19) that w_2 is greater than w_1, i.e., the rill width increases. From that point in the calculations, updated flow velocities, shear stresses, and stream power values can be calculated.

Preliminary calculations showed that it was necessary to place a limit on the decrease in water depth. Thus when the water depth decreases to a limit, $h_{\min}$, it is supposed that no further decrease takes place, i.e.,

$$h_1 + \gamma \Delta z \ge h_{\min} \tag{20}$$

$$w_2 \le w_1 h_1 / h_{\min} \tag{21}$$

3. Methods

3.1. Numerical Formulations

The finite element method (FEM) was used to solve the mathematical models for rill hydraulics and erosion (equations (1), (2), and (6)). We chose to use a sequential strategy for the simulation of the dynamic processes in order to reduce computer storage requirements to a manageable level. In each time step, we treat the variable u in (1), h in (2), and their corresponding derivatives with respect to x as being the known values of the previous time step. Values of u, h, and S for use in (6) are taken as solutions from (1) and (2) for the given time step. The values for h, u, and c are then obtained by solving (1), (2), and (6) sequentially.

With strategy outlined above, numerical formulations of finite element simulation of the processes, for every two-node, linear element, can be given as

$$\frac{\bar{w}^{(e)}L}{6}\begin{bmatrix}2 & 1\\ 1 & 2\end{bmatrix}\left\{\frac{\partial h}{\partial t}\right\} + \left\{\frac{\bar{u}^{(e)}\bar{w}^{(e)}}{2}\begin{bmatrix}-1 & 1\\ -1 & 1\end{bmatrix} + (\bar{u}_x^{(e)}\bar{w}^{(e)} + \bar{u}^{(e)}\bar{w}_x^{(e)})\frac{L}{6}\begin{bmatrix}2 & 1\\ 1 & 2\end{bmatrix}\right\}\{h\} = \frac{\bar{w}^{(e)}L}{6}\begin{bmatrix}2 & 1\\ 1 & 2\end{bmatrix}\{\sigma\} \tag{22}$$

$$\frac{L}{6}\begin{bmatrix}2 & 1\\ 1 & 2\end{bmatrix}\left\{\frac{\partial u}{\partial t}\right\} + \left\{\frac{\bar{u}^{(e)}}{2}\begin{bmatrix}-1 & 1\\ -1 & 1\end{bmatrix} + \frac{\bar{\sigma}^{(e)}L}{6\bar{h}^{(e)}}\begin{bmatrix}2 & 1\\ 1 & 2\end{bmatrix}\right\}\{u\} = -\frac{g}{2}\begin{bmatrix}-1 & 1\\ -1 & 1\end{bmatrix}\{h\} - \frac{g\bar{h}^{(e)}}{4\bar{w}^{(e)}}\begin{bmatrix}-1 & 1\\ -1 & 1\end{bmatrix}\{w\} - \frac{gL}{6}\begin{bmatrix}2 & 1\\ 1 & 2\end{bmatrix}\{\bar{S}_{x0}^{(e)}\{S_x\} + \bar{S}_{fx}^{(e)}\{u_{t-\Delta t}\} - \bar{F}_{Cn}^{(e)}\{n_x\}\} \tag{23}$$

$$\frac{\bar{h}L}{6}\begin{bmatrix}2 & 1\\ 1 & 2\end{bmatrix}\left\{\frac{\partial c}{\partial t}\right\} + \left\{\frac{\bar{u}^{(e)}}{2}\begin{bmatrix}-1 & 1\\ -1 & 1\end{bmatrix} + \frac{\bar{D}_H^{(e)}}{L}\begin{bmatrix}1 & -1\\ -1 & 1\end{bmatrix} + \frac{\bar{\sigma}^{(e)}L}{6\bar{h}^{(e)}}\begin{bmatrix}2 & 1\\ 1 & 2\end{bmatrix}\right\}\{c\} = \frac{L}{6\bar{h}^{(e)}}\begin{bmatrix}2 & 1\\ 1 & 2\end{bmatrix}\{S\} \tag{24}$$

where $\bar{u}^{(e)}$, $\bar{h}^{(e)}$, $\bar{c}^{(e)}$, $\bar{w}^{(e)}$, $\bar{\sigma}^{(e)}$, $\bar{D}_H^{(e)}$, $\bar{u}_x^{(e)}$, $\bar{w}_x^{(e)}$, $\bar{S}_{x0}^{(e)}$, $\bar{S}_{fx}^{(e)}$, and $\bar{F}_{Cn}^{(e)}$ are the averages of the corresponding variables within the element e and L is the element length.

These three equations can be represented by one general equation as

$$[p^{(e)}]\{\dot{\phi}\} + [k^{(e)}]\{\phi\} - \{f^{(e)}\} = \{0\} \tag{25}$$

where $\{\phi\}$ is $\{h\}$, $\{u\}$, or $\{c\}$, and $[p]$, $[k]$, and $\{f\}$ are the capacitance matrix, the stiffness matrix, and the force vector in each equation and element.

The system of equations expressed by (22), (23), and (24) are a system of ordinary differential equations with respect to time. The "time marching" integral method can be used to obtain the solutions for different time steps. For this purpose, finite difference in time was used.

Assembling the local matrices, we obtain a system of equations for solving the problem, with the global matrix $[A]$ and global vector $\{B\}$ specified as

$$[A]\{\phi\} = \{B\} \tag{26}$$

$$[A] = \sum_{e=1}^{N} (p + \theta \Delta t [k^{(e)}]) \tag{27}$$

$$\{B\} = \sum_{e=1}^{N} ([p^{(e)}] - (1 - \theta)\Delta t[k^{(e)}])\{\phi\}_t + \Delta t\{f^{(e)}\} \quad (28)$$

where $\theta = 0, \frac{1}{2}, 1$ for differential patterns in time.

3.2. Computational Procedures

The framework of program is outlined as the following:

1. Data for initial and boundary conditions for elevations, widths, error limits for velocity, water depth, and sediment concentration are read, along with soil information such as tensile strength and its variation.
2. The hydraulic equations for mass and momentum balance (equations (1) and (2)) are solved for velocity and water depth.
3. Transport capacity is computed (equation (9)).
4. Detachment or deposition rates are calculated, depending upon whether sediment load is less than or greater than transport capacity (equations (11) and (12)).
5. The sediment continuity equation is solved for sediment concentration (equation (6)).
6. Errors for velocity, water depth, and sediment concentration, as compared to the corresponding values at the previous time step, are calculated. If one or more of the errors are greater than the set values, we return to item 2 (above) for another iteration. If any of the three errors is greater than that for the previous iteration, the time increment for the calculation is shortened. The initial time step is 50 s and may go as short as 0.5 s, depending upon the number of interations where the time step is decreased. Otherwise, the same time increment is kept for the next iteration. If the errors are all in the satisfactory range, we continue to the next part (7) of the calculations.
7. Elevational changes are calculated from the sediment source rate, i.e., detachment or deposition (equation (15)).
8. Width evolutions from deposition are calculated (equation (19)).
9. Rill slopes are calculated from the newly obtained elevation values (equation (5)).
10. Time steps are checked. If the desired number of time steps or end of simulation is reached, stop. Otherwise, go back to step 2 for the next time step.

3.3. Flume Experiments

A flume of approximately 8.5 m long and 0.6 m wide was used for the experiments. The slope of the flume was adjustable. Cecil soil, a kaolinitic, sandy-clay loam, air dried then sieved, was packed into the flume to an even depth of 20 cm to imitate a uniformly sloped bed of homogeneous soil. A slight "V" was shaped on the surface over the cross section of the bed to ensure that water did not tend toward the outer edges of the flume along its length. Experiments were made on three initial slopes: 3, 5, and 7%. Clear water was introduced onto the upper end of the bed. Water inflow rates of 7.6, 11.4, and 15.2 L min^{-1} were used for each of the three slopes.

At each flow rate and slope, velocities and rill widths along the rill and sediment concentration at the outlet were measured after the water flow was established. Velocities were measured with fluorescent dye [*King and Norton*, 1992; *Gilley et al.*, 1990]. Velocity measurements at five contiguous sections along the rill and two or three sediment samples were taken from the outlet for each treatment. Rill widths were recorded at each 30 cm interval.

Reynold's numbers of the flow ($Re = u\,h/\nu$) ranged from approximately 400 to 5700, with 93% in the range greater than 500, 68% greater than 1000, and 33% greater than 2000. Generally, it is considered that channel flows with Re less than 500 are laminar, from 500 to 2000 fall in the transitional range, and those greater than 2000 are fully turbulent [*Chow*, 1959]. This classification is questionable for rill flows wherein flow depths are small compared to the roughness element sizes [see, e.g., *Bunte and Poesen*, 1993]. In our case, flow depths ranged of the order of 1 to 10 mm and exhibited significant variations in flow depth along the rill for the same experimental treatment.

3.4. Boundary and Initial Conditions

Considering the experimental setup, the boundary conditions for simulating the processes in the examples are listed as

$$u_{X_0} = u_0$$
$$h_{X_0} = h_0$$
$$c_{X_0} = 0 \quad (29)$$
$$\left.\frac{\partial c}{\partial x}\right|_{x=X_0} = \frac{S_{ss}(0, t)}{u(0, t)h(0, t)}$$

where u_0, h_0, and $S_{ss}(0, t)$ are velocity, water depth, and sediment source at the inlet. The parameters u_0 and h_0 are restricted by the rate (q) of in-flow as

$$q = u_0 h_0 w_0$$

where w_0 is the width at the inlet.

The initial conditions are given as

$$u_{x_i}(x, t = 0) = u_i$$
$$h_i(x, t = 0) = h_i \quad (30)$$
$$c_i(t = 0) = 0$$

and u_i and h_i can be set at any value, except that h_i may not be zero for use in (3).

3.5. Material Parameters

3.5.1. Detachment rate coefficient for the probability function. In order to apply the probabilistic detachment model to the flume data it was necessary to determine the detachment model parameters. Parameters for the detachment model had been previously obtained using point detachment data [*Nearing*, 1991], but not for the Cecil soil. *Nearing et al.* [1991a] did measure point detachment for the Cecil soil, however. The data from that study were analyzed and used here to parameterize the detachment model. Optimization of parameters was conducted as suggested by *Nearing* [1991] and values obtained were as follows: the coefficient of variation of T, CV_T, was set at 0.4; the coefficient of variation of τ, CV_τ, was set also at 0.4; and the parameter K from (8) was optimized to a value of 440.54 kg m^{-3}. Average tensile strength, T, was taken to be 1100 Pa, as was measured by *Nearing et al.* [1991b]. These parameters produced a coefficient of determination, r^2, of 0.998 between calculated (equation (8)) and measured [*Nearing et al.*, 1991a] point detachment rates.

3.5.2. β: First-order deposition parameter. In sections of the rill where sediment load was higher than the transport capacity of the flow, the sediment sink term in (6) was calculated as a first-order function of the sediment load excess:

$$\partial c^*/\partial t = -\beta c^* \quad (31)$$

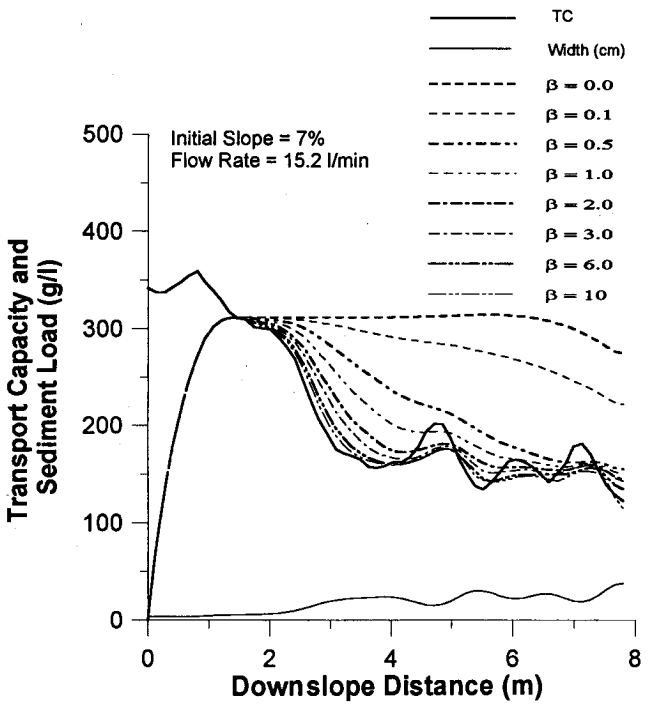

Figure 2. Analysis of the first-order deposition coefficient, β, for the case of 5% slope and flow rate of 11.4 L min^{-1}.

where β (s^{-1}) is a first-order, empirical, deposition parameter and c^* (kg m^{-3}) is excess sediment concentration, i.e., $c^* = c - c_{tc}$, where c_{tc} is the sediment concentration at transport capacity. Numerical tests on the influence of different β values on deposition were conducted and the results are shown in Figure 2 for the case of constant, nonuniform rill width and constant slope. Flow rate used was 15.2 L min^{-1} and initial bed slope was 7%. The appropriate value for β must produce a pattern of deposition such as was observed in the rill; thus from Figure 2 we determined that the appropriate β value for these experiments will fall into the range from 1 to 6. Further study is necessary to determine the best value of β in different situations, but for purposes of this study we consider that using a value of $\beta = 3$ was reasonable for our experimental conditions.

3.5.3. D_x: Hydrodynamic dispersion coefficient of sediment. The hydrodynamic dispersion coefficient of sediment is another important parameter in the sediment continuity equation given by (6). Various D_x values were tested so as to determine the sensitivity of the calculations to D_x and to select an appropriate value. The results, as given in Figure 3 for the case of varied rill width with constant slope, show that D_x ranging from 0.01 to 0.1 m^2 s^{-1} gave reasonable results, i.e., sediment load changes downslope followed the pattern of deposition observed in the rill. Flow rate used was 15.2 L min^{-1} and initial bed slope was 7%. From Figure 3 we see that the sections of the sediment load curve which exhibit increasing sediment load intersect with the decreasing transport capacity curve, whereupon the sediment load decreases as expected. As with the case of the deposition coefficient, the optimal value for D_x should be further studied with explicit experimental data, but a D_x of 0.01 to 0.1 m^2 s^{-1} was apparently reasonable for the given conditions. A value of 0.05 m^2 s^{-1} for D_x was chosen for this study.

3.6. Simulation Scenarios

We wrote the mathematical model and its finite element solution in the form of a C++ program. For initial evaluation of the model we compared model-computed velocities and sediment concentrations to the measured data. Calibrations were made as necessary. In order to investigate the spatial and temporal evolution patterns of the rills we then performed simulation for increasingly complex scenarios: (1) time invariant and spatially uniform rill widths and bed slopes (elevations); (2) time invariant and spatially uniform widths, time variable and spatially nonuniform slopes; (3) time invariant but spatially nonuniform widths and time variable and spatially nonuniform slopes; (4) time variable and spatially nonuniform rill widths and bed slopes.

Simulations were conducted for three constant inflow rates of 7.6, 11.4, and 15.2 L/min^{-1} (2, 3, and 4 gallons per minute) and each for three initial bed slopes of 3, 5, and 7%.

4. Results and Discussion

4.1. Comparisons of Simulations and Experiments

We made comparisons between experimental and simulated data using the case of constant and nonuniform, measured rill widths and constant slopes. Velocities were measured as averaged values in each of five sections of equal lengths of the rill. Sediment concentrations were averaged from the two or three samples for each treatment.

Simulated velocities, as regressed, were nearly on a one-to-one line with the experimental values, with $r^2 = 0.6185$ (Figure 4).

Initial simulations showed a problem with the sediment transport equation used in the model as applied to these data (Figure 5). The model initially underpredicted sediment loads. The reason for this may be simply that while the sediment transport equation worked well in the study of *Nearing et al.* [1997] on the log-log scale, a factor of 3 difference for any individual data set is not unreasonable for this type of data. We calibrated the sediment transport equation to the data in this

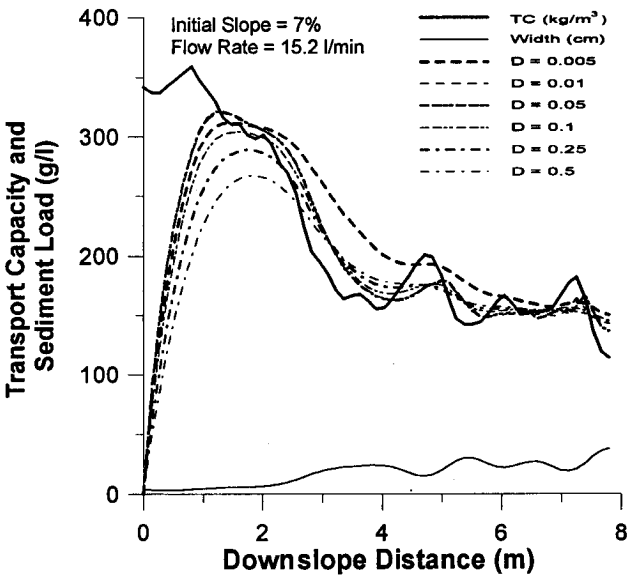

Figure 3. Analysis of the hydrodynamic dispersion coefficient, D_x, for the case of 5% slope and flow rate of 11.4 L min^{-1}.

experiment by simply increasing the sediment transport function (equation (9)) by a factor of 2.71.

Sediment results for the calibrated model are shown in Table 1. The model followed the trends in the measured data quite well. Sediment concentrations increased as a function of bed slope for both the measured and simulated data. The trends in sediment concentration as a function of flow rate were not as definite. For the 3 and 7% slopes the 15.2 L min^{-1} flow rate showed a lower measured sediment concentration than did the 11.4 L min^{-1} flow rate. The model also showed a similar trend for the 7% slope and showed nearly similar (31.5 versus 32.6 g L^{-1}) concentrations for the 3% slope case for the 11.4 and 15.2 L min^{-1} flow rates, respectively. This result illustrates the fact that hydraulics was the controlling influence over erosion in the flume rather than flow rate per se. In these cases the wider flow near the outlet of the flume for the 15.2 L min^{-1} case lowered the transporting capacity to a level near or less than that for the 11.4 L min^{-1} case. The effect is more or less random, in the sense that wider and narrower regions of the rill flow alternated along the flume length, and it so happened that the rill was wider at the flume end for the 15.2 L min^{-1} flow rate case for the 3 and 7% slope as compared to the 11.4 L min^{-1} case. This result illustrates the importance of spatial variability of flow patterns in apparent random variations of soil erosion measurements.

4.2. Time Invariant and Spatially Uniform Rill Widths and Bed Slopes

For these trials feedback between soil detachment, changes in bed morphology, and hydraulics were not allowed, which are the implicit assumptions heretofore used in erosion modeling [*Nearing et al.*, 1989, 1990; *Morgan et al.*, 1992; *Morgan*, 1995; *Misra and Rose*, 1996]. When constant flow rate is introduced into the rill, water depth and velocity after some period of time are simulated as both constant and uniform, and hence sediment transport capacity is also uniform and constant (Figure 6a). The sediment load increases downslope gradually and approaches the transport capacity. Likewise, detachment rate decreases along the rill as the sediment load increases (Figure 6b), i.e., detachment rate is not uniform along the rill. This is due to the sediment feedback relationship as discussed above wherein detachment rate is inversely proportional to the sediment load deficit with respect to transport capacity. If one were to calculate the amount of sediment removed from the bed over a period of time, the results would indicate a greater loss of rill bed material at the upper end of the rill than at the lower end (Figure 6c). This case is obviously nonsensical in terms of sediment mass balance and the assumption of constant slope along the rill, and the results illustrate a fundamental problem and limitation associated with current rill and flow detachment erosion models which do not take into account changes in bed slope as erosion progresses.

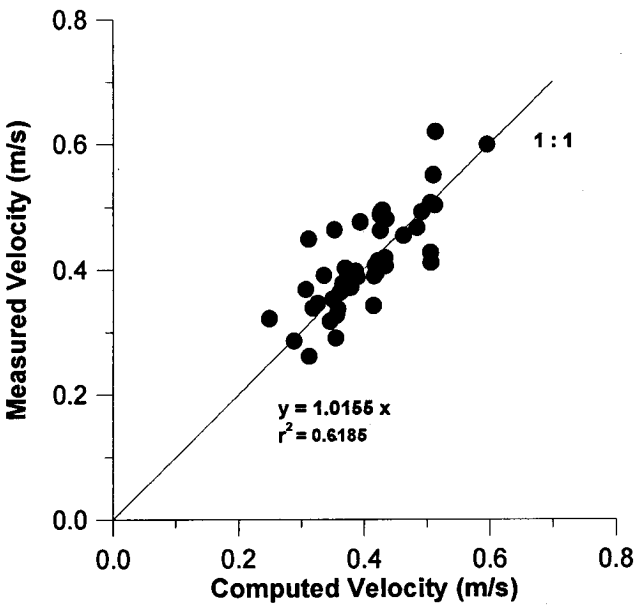

Figure 4. Measured and computed average flow velocities.

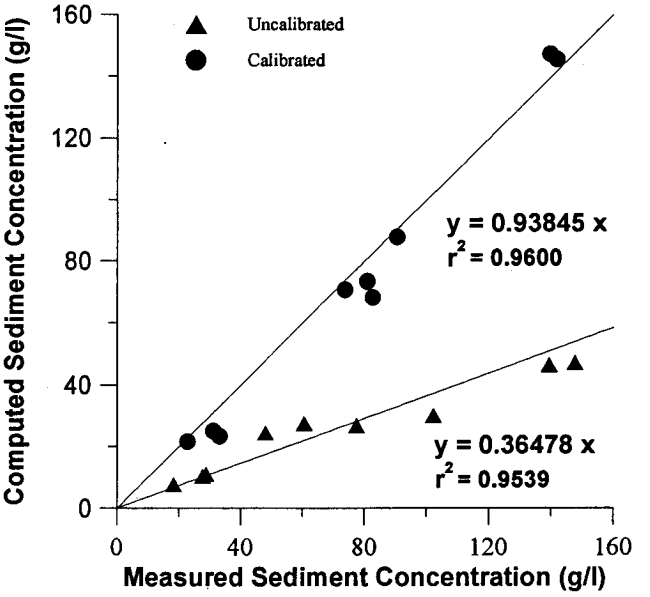

Figure 5. Measured and computed sediment concentrations for the calibrated and uncalibrated simulations.

4.3. Time Invariant and Spatially Uniform Widths and Time Variable and Spatially Nonuniform Slopes

This case considers the influence of detachment and deposition on changes and variations of rill bed slope, as well as the influence of bed slope changes on the rill hydraulics and the further influence of the hydraulics on detachment rates. It does not, however, take into consideration variabilities in flow width either in time or space. Initially, the transport capacity, detachment rate, and elevation on the rill bed are the same as for the

Table 1. Sediment Concentrations From the Model Calculations and the Measured Flume Data

Flow Rate, L min^{-1}	Slope, %	Sediment Concentrations, g L^{-1}	
		Computed	Measured
7.6	3	19.77	18.20
11.4	3	31.45	28.70
15.2	3	32.59	27.60
7.6	5	59.63	54.78
11.4	5	68.62	60.45
15.2	5	76.85	81.00
7.6	7	79.18	102.25
11.4	7	139.21	147.52
15.2	7	130.74	139.30

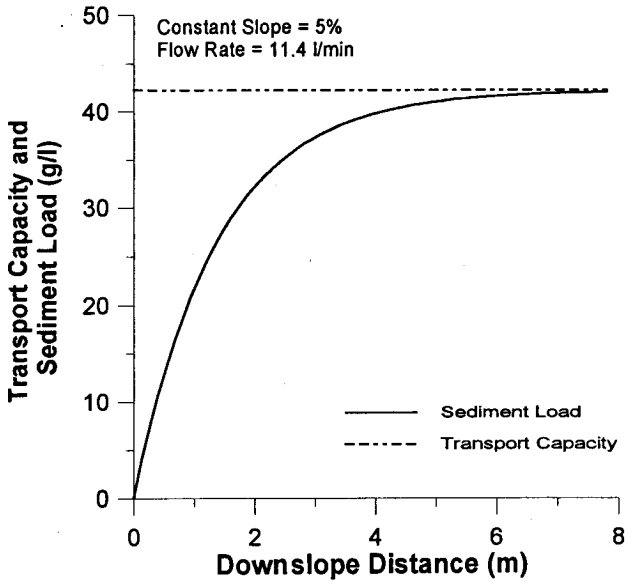

Figure 6a. Simulated transport capacity and sediment load results for time invariant and spatially uniform rill widths and bed elevations. Flow rate was 11.4 L/min and initial bed slope was 5%.

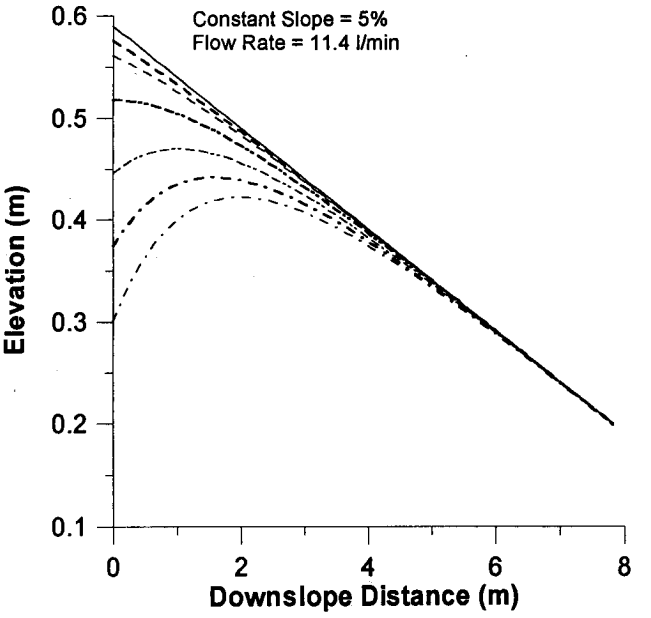

Figure 6c. Same as Figure 6a, except for bed elevations.

previous case (Figures 7a, 7b, and 7c). Transport capacity is constant along the bed length (Figure 7a), detachment rate is maximum at the upper end of the bed where clear water enters, and decreases to a very low value at the end of the bed (Figure 7b), and the slope is uniform and constant with distance (Figure 7c). As time progresses, however, material is eroded at a greater rate from the upper end of the flume and the bed slope changes (Figure 7c). The rill bed becomes flatter near the upper end, and the flattening extends farther downslope with time. This effects a corresponding change in the flow hydraulics, which translates to a change in both sediment transport capacity (Figure 7a) and soil detachment rate (Figure 7b) along the rill bed. Whereas during the initial stages of rill erosion the detachment rate is greatly different along the bed, the detachment rate after 83 min (in this case) is significantly more homogeneous along the rill.

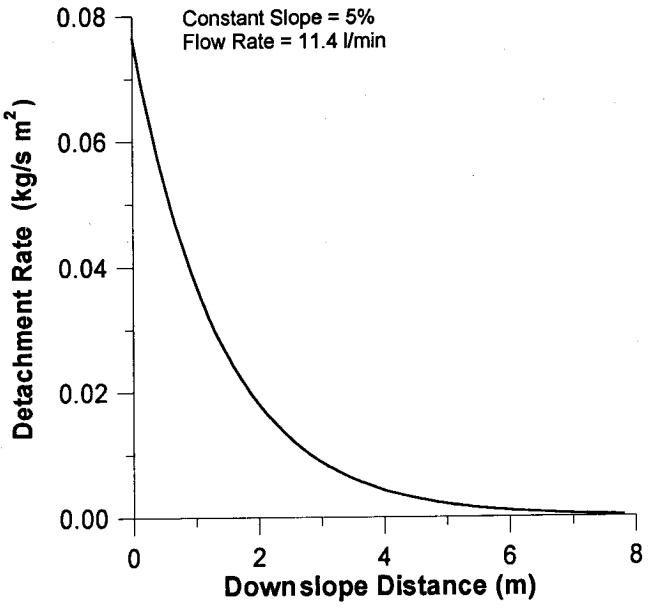

Figure 6b. Same as Figure 6a, except for detachment rates.

4.4. Time Invariant but Spatially Nonuniform Widths and Time Variable and Spatially Nonuniform Slopes

In this case, the rill width is kept constant with respect to time but is nonuniform; namely, the experimentally measured widths along the rill are used. This case addresses the complexity and physical reality of spatial variability associated with rill flow hydraulics and morphology. Rill bed evolution in terms of changes in the bed elevation and slope is computed as a

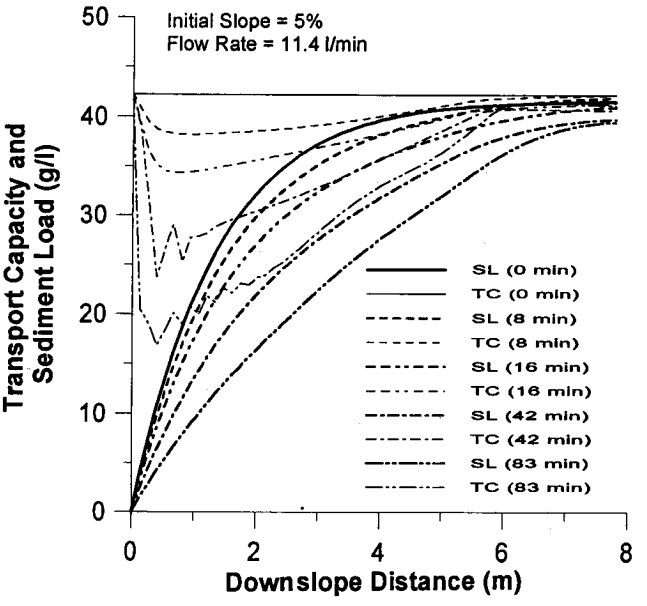

Figure 7a. Simulated transport capacity and sediment load results for time invariant and spatially uniform widths and time variable and spatially nonuniform bed elevations. Flow rate was 11.4 L min^{-1} and initial bed slope was 5%.

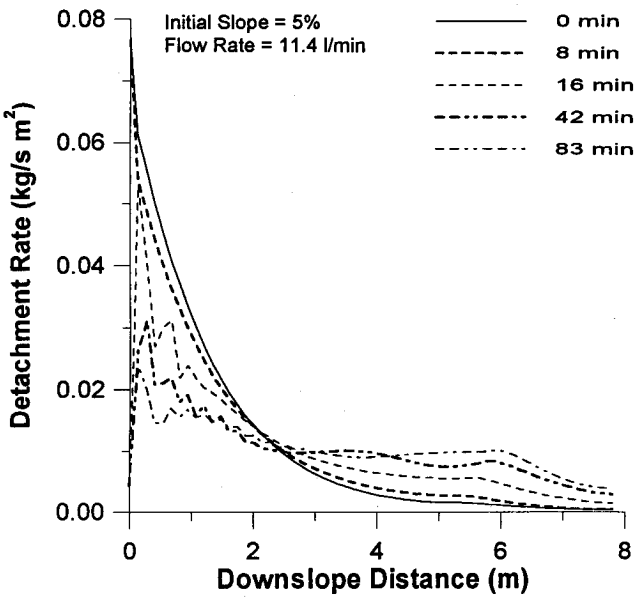

Figure 7b. Same as Figure 7a, except for detachment rates.

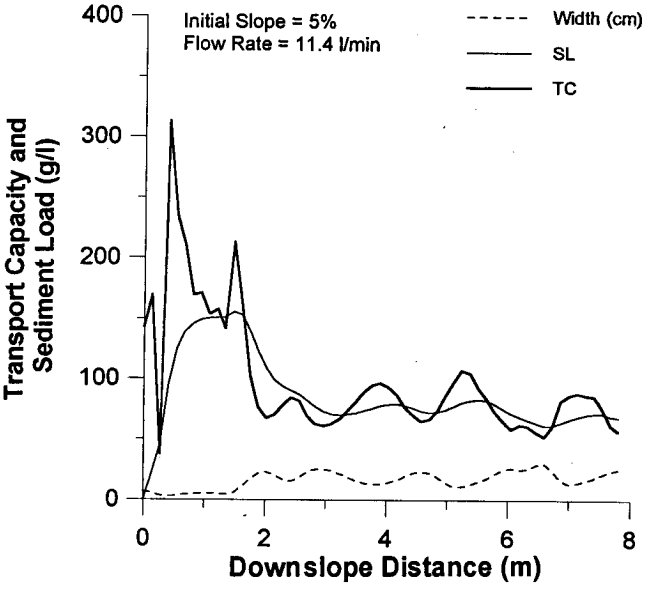

Figure 8a. Simulated transport capacity and sediment load results for time invariant and spatially nonuniform widths and time variable and spatially nonuniform bed elevations. Flow rate was 11.4 L min^{-1} and initial bed slope was 5%.

result of detachment and deposition, along with the changes in hydraulics and subsequent erosion along the bed.

Results for a flow rate of 11.4 L min^{-1} and slope of 5% are illustrated in Figures 8a, 8b, and 8c. Transport capacity varies along the rill bed largely as a function of the rill width initially (Figure 8a) and later in the experiment according to both rill width and local bed slope. Where the rill is narrow, transport capacity is greater, and vice versa. The variations are quite large. For these results computed sediment transport capacity dropped from approximately 210 to 70 kg/m^3 in the distance from 1.5 to 2 m rill length (Figure 8a). The abrupt changes were even greater for the 3% slope, though less for the 7% slope (results not shown).

The sediment load tends to follow, but lag, the downslope variability in the sediment transport capacity. The sediment load curves are somewhat damped relative to the transport curves, however, and the downslope variability of the load is not as great as that of the transport capacity. This is due to the fact that within the model, detachment and deposition are first-order functions of the difference between transport capacity and sediment load, with the added factor of sediment dispersion. Whereas sediment transport capacity dropped from 210 to 70 kg/m^3 between 1.5 and 2 m for 5% case (Figure 8b), as discussed above, calculated sediment load dropped only from 160 to 120 kg/m^3 over the same distance.

Associated with the fluctuations in the sediment transport capacity and sediment load is the fact that the rill has alternating regions of detachment and deposition (Figure 8a). This result was observed visually in the flume during the experi-

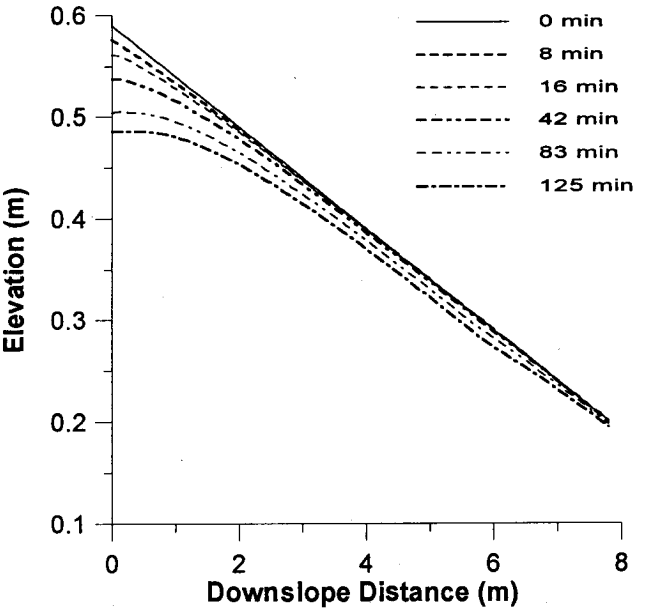

Figure 7c. Same as Figure 7a, except for bed elevations.

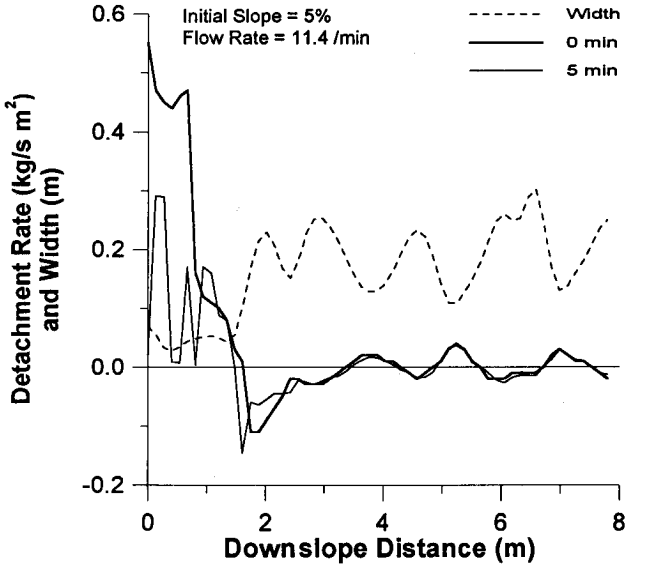

Figure 8b. Same as Figure 8a, except for detachment rates.

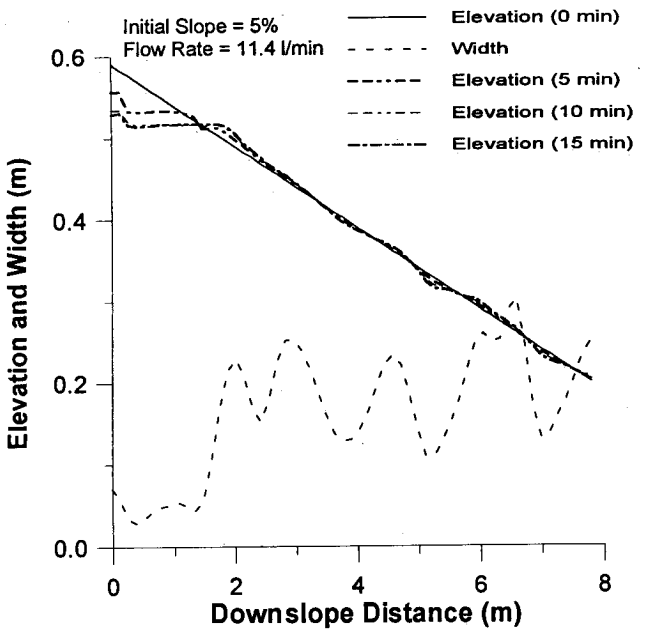

Figure 8c. Same as Figure 8a, except for bed elevations.

ments. The narrow areas of the rills were apparently scouring the surface, while the wider regions were experiencing sediment deposition, and the two types of regions alternated down the rill length. The previous cases discussed above where rill width was modeled as being spatially uniform do not exhibit this phenomenon and, in fact, do not allow for net deposition at any point along the rill bed (Figures 6b and 7b).

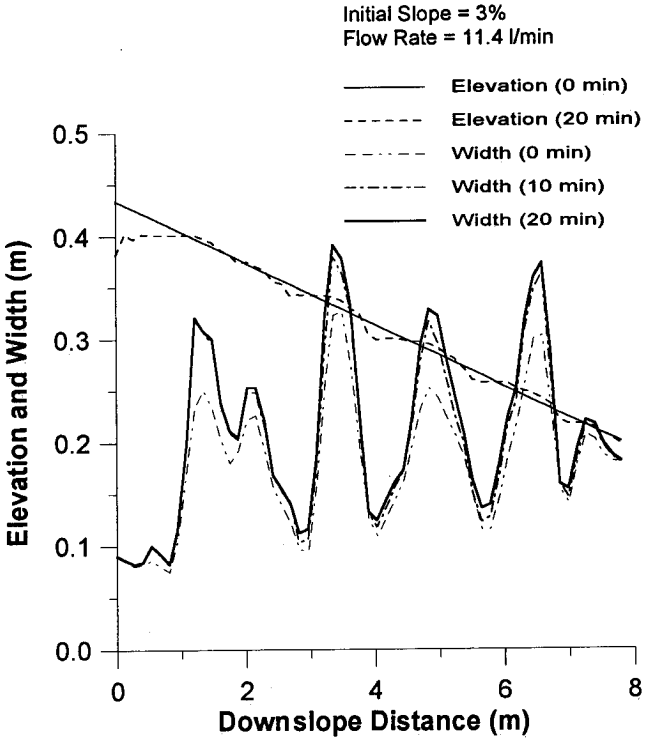

Figure 9a. Simulated rill widths as a function of time for the case of time variable and spatially nonuniform rill widths and bed elevations for a flow rate of 11.4 L/min and 3% initial slope.

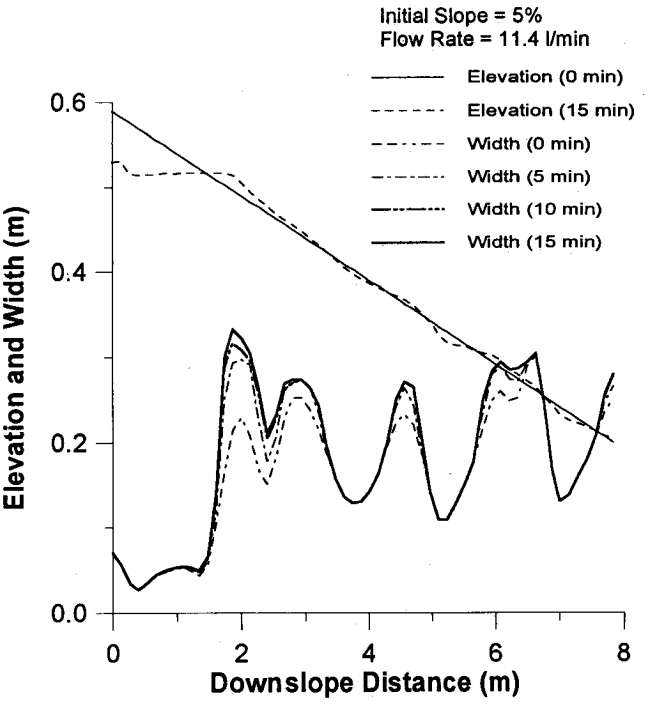

Figure 9b. Same as Figure 9a, except for 5% initial slope.

4.5. Time Variable and Spatially Nonuniform Rill Widths and Bed Slopes

This case takes into account a further complexity of rill evolution associated with the widening of the rill as deposited material accumulates on the bed in the regions of deposition. Deposition of sediment tends to increase the rill width and in turn decrease both the flow velocity, depth, and transport capacity, which further enhances deposition. In other words, once a deposition region is initiated, it may act as a self-propagating phenomenon until it is limited by a minimum flow depth. An effort was made here to simulate the width evolution as influenced by sediment deposition. Results are illustrated in Figures 9a, 9b and 9c for flow rate 11.4 L min^{-1} and slopes of 3, 5, and 7%, respectively. The initial rill widths are the experimentally measured ones as adopted for the previous case discussed above and then allowed to evolve as deposition proceeds. The computed rill width increased in the depositional region, thus illustrating computationally the concept for rill widening discussed above.

The rules for evolution of the rill width in this model are limited to the case of rill widening in areas of deposition, but the results are encouraging. More work is needed to better define the limiting factors for rill widening and also for the process of "rechanneling" to describe the rill scouring process downstream of the depositional areas.

5. Summary

Rilling is a critical aspect of soil erosion and sediment transport in upland areas. Therefore, to understand soil erosion processes in a rill is of significance. Mathematical modeling, in combination with controlled laboratory experiments (i.e., physical modeling), is one path toward a better understanding of the rill. This study presents a mathematical representation of the rill which is quite different from previous models in several ways. This is a first attempt to develop an evolutionary model

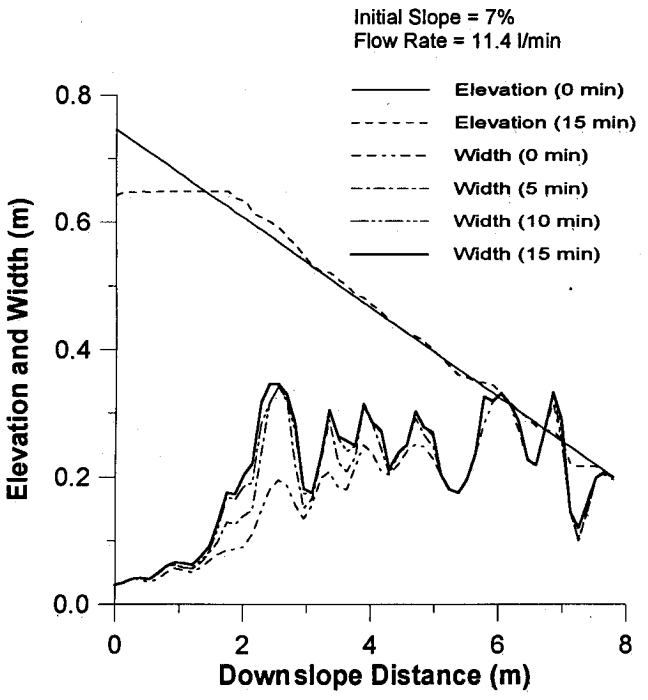

Figure 9c. Same as Figure 9a, except for 7% initial slope.

which "self-generates" changes in the rill morphology over time and space. In addition to being a dynamic and a spatially varied model, it links hydraulics, sediment redistribution, and bed morphology in a dynamic feedback loop. The equations allow for bed elevations and rill flow widths to change at varying rates along the rill length as a function of erosional processes.

In addition to the evolutionary aspect of the mathematical model here presented, the equations also contain other new characteristics which better describe the physics of the rill. Although we know that turbulence is an integral and necessary condition for detachment by flowing water [*Nearing and Parker*, 1994], and though the physics of the turbulent detachment process is partially understood [*Nearing*, 1991], turbulence has not been specifically integrated into a working erosion model as is done here. Also, the inclusion of the term in the sediment continuity equation for sediment dispersion allows for new theoretical exploration of that factor.

Limitations of the model are evident. Certainly one-dimensionality places limits on the cross-sectional variability in the rill structure and processes. Meandering is not modeled. Although the model has capability of addressing many aspects of soil erosion by water, further study as how to incorporate headcuts, sidewall sloughing, width changes and stabilization during scour, and rill narrowing as it leaves depositional regions would enhance the model's usefulness. The limitation of the model relative to channel width adjustments is arguably the weakest link in the model structure. Better knowledge of the processes involved in rill width adjustments is needed. Also, we need better data on the rates of rill width changes in order to better evaluate the model's predictions of morphological evolution. As was mentioned previously, parameter values for the sediment deposition (β) and dispersion (D_x) terms need to be physically defined based on direct experimental measurements. In the current study, these values were determined solely by conducting sensitivity analyses on the parameters and choosing reasonable values (Figures 2 and 3). Experiments and analysis are also needed in order to understand why we needed to introduce arbitrary values for minimum flow depth, h_{min}, in the hydraulic calculations.

Despite these limitations, the model results point to some interesting and clear implications. The simulations indicate that in a rill with uniform initial conditions, including uniform initial bed slope and uniform flow rate on a homogeneous soil bed, random variations in rill width can cause variances in transport capacity which cause differences in the source term of the sediment continuity equation over time. The model results for rill widening suggest that once the wider areas of the rill begin to form, deposition is enhanced and the wide areas become wider. Detachment regions remain narrow, which is conducive to detachment. Thus the rill does not tend toward a uniform system but rather to one of alternating regions of detachment and deposition which are self-propagating.

The fact that both sediment transport capacity and sediment load vary in considerable amounts down the rill has significant implications for field and laboratory measurements of erosion. The results of this study imply that significant differences will be obtained in sediment measurements even under very controlled environmental (soil, moisture, slope, flow rate, etc.) conditions. In other words, if we measure erosion from field plots, for example, we can expect that there will be a significant degree of variation between replicated plots which cannot and should not be explained in terms of differences in the plot characteristics. Some of the variation in replicated plots must be due to random variations in flow patterns and erosional distribution patterns in the rills on the plots. This degree of natural variation should be expected and planned in setting up erosion monitoring systems and in interpreting the results of field studies. It might be expected, for example, that all erosion simulation models when applied to field erosion data will exhibit a degree of uncertainty which cannot be explained or removed by "better" characterization of the erosion plot and its inputs.

Another implication of this study is the uncertainty of current erosion prediction in terms of the spatial variation of erosion on hillslopes. The WEPP model, for example, portends to provide estimates of erosion rates along a hillslope profile [*Flanagan and Nearing*, 1995]. The results shown in this numerical study of rill erosion indicate that the spatial distribution estimates from the WEPP and other models, which assume no feedback between erosion and bed morphology, may be in error.

References

Bunte, K., and J. Poesen, Effects of rock fragment covers on erosion and transport of noncohesive sediment by shallow overland flow, *Water Resour. Res.*, *29*, 1415–1424, 1993.

Chow, V. T., *Open-Channel Hydraulics*, McGraw-Hill, New York, 1959.

Einstein, H. A., and Ning Chien, Second approximation to the solution of the suspended load theory, report, Fluid Mech. Lab., Univ. of Calif., Berkeley, 1954.

Elliot, W. J., A process based rill erosion model, Ph.D. dissertation, Iowa State Univ., Ames, 1988.

Elliot, W. J., and J. M. Laflen, A process-based rill erosion model, *Trans. ASAE*, *36*, 65–72, 1993.

Elliot, W. J., A. M. Liebenow, J. M. Laflen, and K. D. Kohl, A compendium of soil erodibility data from WEPP cropland soil field erodibility experiments 1987 & 88, *NSERL Rep. 3*, Natl. Soil Erosion Res. Lab., West Lafayette, Indiana, 1989.

Ellison, W. D., Soil erosion studies, part VI, Soil detachment by surface flow, *Agric. Eng.*, *28*, 402–405, 1947.

Flanagan, D. C., and M. A. Nearing, USDA-Water Erosion Prediction Project: Hillslope profile and watershed model documentation, *NSERL Rep. 10*, Natl. Soil Erosion Res. Lab., West Lafayette, Indiana, 1995.

Foster, G. R., Modeling the erosion process, in *Hydrologic Modeling of Small Watersheds*, edited by C. T. Haan, pp. 295–380, Am. Soc. of Agric. Eng., St. Joseph, Mich., 1982.

Foster, G. R., and L. D. Meyer, A closed form erosion equation for upland areas, in *Sedimentation (Einstein)*, edited by H. W. Shen, pp. 12.1–12.9, Colo. State Univ., Ft. Collins, 1972.

Gilley, J. E., E. R. Kottwitz, and J. R. Simanton, Hydraulic characteristics of rills, *Trans. ASAE*, *33*, 1900–1906, 1990.

Govers, G., Empirical relationships for the transport capacity of overland flow, in *Erosion, Transport, and Deposition Processes, Proceedings of Jerusalem Workshop, Jerusalem, Israel, March–April 1987*, *IAHS Publ., 189*, 45–63, 1990.

Govers, G., Relationship between discharge, velocity, and flow area for rills eroding loose, non-layered materials, *Earth Surf. Processes Landforms*, *17*, 515–528, 1992.

Govers, G., and G. Rauws, Transporting capacity of overland flow on plane and on irregular beds, *Earth Surf. Processes Landforms*, *11*, 515–524, 1986.

Hairsine, P. B., and C. W. Rose, Modeling water erosion due to overland flow using physical principles, 1, Sheet flow, *Water Resour. Res.*, *28*, 237–243, 1992a.

Hairsine, P. B., and C. W. Rose, Modeling water erosion due to overland flow using physical principles, 2, Rill flow, *Water Resour. Res.*, *28*, 245–250, 1992b.

Jayawardena, A. W., and J. K. White, A finite element distributed catchment model, I, Analytical basis, *J. Hydrol.*, *34*, 269–286, 1997.

King, K. W., and L. D. Norton, Methods for rill flow velocity dynamics, *Pap. 92-2542*, Am. Soc. of Agric. Engr., St. Joseph, Mich., 1992.

Laflen, J. M., W. J. Elliot, R. Simanton, S. Holzhey, and K. D. Kohl, WEPP soil erodibility experiments for rangeland and cropland soils, *J. Soil Water Conserv.*, *46*(1), 39–44, 1991.

Meyer, L. D., G. R. Foster, and S. Nikolov, Effect of flow rate and canopy on rill erosion, *Trans. ASAE*, *18*, 905–911, 1975.

Milne-Thomson, M. C. B. E., *Theoretical Hydrodynamics*, Macmillan, Indianapolis, Indiana, 1960.

Misra, R. K., and C. W. Rose, Application and sensitivity analysis of process based erosion model GUEST, *Eur. J. Soil Sci.*, *47*, 593–604, 1996.

Morgan, R. P. C., The European soil erosion model: An update on its structure and research base, in *Conserving Soil Resources, European Perspectives*, edited by R. J. Rickson, pp. 286–299, CAB Int., Wallingford, England, 1995.

Morgan, R. P. C., J. N. Quinton, and R. J. Rickson, EUROSEM documentation manual, Silsoe College, Silsoe, Bedford, England, 1992.

Nearing, M. A., A probabilistic model of soil detachment by shallow turbulent flow, *Trans. ASAE*, *34*, 81–85, 1991.

Nearing, M. A., and A. D. Nicks, Evaluation of the Water Erosion Prediction Project (WEPP) model for hillslopes, in *Modelling Soil Erosion by Water*, edited by J. Boardman and D. T. Favis-Mortlock, *NATO ASI Ser., Ser. I*, *55*, 45–56, 1998.

Nearing, M. A., and S. C. Parker, Detachment of soil by flowing water under turbulent and laminar conditions, *Soil Sci. Soc. Am. J.*, *58*, 1612–1614, 1994.

Nearing, M. A., G. R. Foster, L. J. Lane, and S. C. Finkner, A process-based soil erosion model for USDA-water erosion prediction project technology, *Trans. ASAE*, *32*, 1587–1593, 1989.

Nearing, M. A., L. J. Lane, E. E. Alberts, and J. M. Laflen, Prediction technology for soil erosion by water: status and research needs. *Soil Sci. Soc. Am. J.*, *54*, 1702–1711, 1990.

Nearing, M. A., J. M. Bradford, and S. C. Parker, Soil detachment by shallow flow at low slopes, *Soil Sci. Soc. Am. J.*, *55*, 339–344, 1991a.

Nearing, M. A., S. C. Parker, J. M. Bradford, and W. J. Elliot, Tensile strength of thirty-three saturated repacked soils, *Soil Sci. Soc. Am. J.*, *55*, 1546–1551, 1991b.

Nearing, M. A., L. D. Norton, D. A. Bulgakov, G. A. Larionov, L. T. West, and K. M. Dontsova, Hydraulics and erosion in eroding rills, *Water Resour. Res.*, *33*, 865–876, 1997.

Rose, C. W., J. R. Williams, G. C. Sander, and D. A. Barry, A mathematical model of soil erosion and deposition processes, I, Theory for a plane land element, *Soil Sci. Soc. Am. J.*, *47*, 991–995, 1983a.

Rose, C. W., J. R. Williams, G. C. Sander, and D. A. Barry, A mathematical model of soil erosion and deposition processes, II, Application to data from an arid-zone catchment, *Soil Sci. Soc. Am. J.*, *47*, 996–1000, 1983b.

Shames, I. H., *Mechanics of Fluids*, 3rd ed., McGraw-Hill, New York, 1992.

Vanoni, V., and G. N. Namicos, Resistance properties of sediment-laden strains, *Trans. ASCE*, *125*, 30–55, 1960.

Wendt, R. C., E. E. Alberts, and A. T. Hjemfelt Jr., Variability of runoff and soil loss from fallow experimental plots, *Soil Sci. Soc. Am. J.*, *50*, 730–735, 1986.

Zienkiewicz, O. C., and R. L. Taylor, *The Finite Element Method*, vol. 2, *Solid and Fluid Mechanics, Dynamics and Non-linearity*, 4th ed., McGraw-Hill, New York, 1991.

V. F. Bralts and K. Haghighi, Agricultural and Biological Engineering Department, Purdue University, West Lafayette, IN 47907.

T. Lei and M. A. Nearing, USDA-ARS National Soil Erosion Research Laboratory, 1196 Soil Building, West Lafayette, IN 47907-1196. (e-mail: nearing@ecn.purdue.edu)

(Received December 4, 1997; revised June 23, 1998;
accepted June 26, 1998.)